Journal of Alloys and Compounds 584 (2014) 363–368

Contents lists available at ScienceDirect

Journal of Alloys and Compounds

journal homepage: www.elsevier.com/locate/jalcom

Impacts of Ni–Co substitution on the structural, magnetic and dielectric properties of magnesium nano-ferrites fabricated by micro-emulsion method

Rajjab Ali [a], Azhar Mahmood [a], Muhammad Azhar Khan [b,*], Adeel Hussain Chughtai [c], Muhammad Shahid [d], Imran Shakir [e], Muhammad Farooq Warsi [a,*]

[a] Department of Chemistry, The Islamia University of Bahawalpur, Bahawalpur 63100, Pakistan
[b] Department of Physics, The Islamia University of Bahawalpur, Bahawalpur 63100, Pakistan
[c] Institute of Chemical Sciences, Bahauddin Zakaryia University, Multan 6100, Pakistan
[d] BK 21 Physics Research Division, Institute of Basic Sciences, SKKU Advanced Institute of Nanotechnology, Department of Energy Science, Sungkyunkwan University, Suwon 440-746, South Korea
[e] Deanship of Scientific Research, College of Engineering, King Saud University, PO Box 800, Riyadh 11421, Saudi Arabia

ARTICLE INFO

Article history:
Received 7 July 2013
Accepted 16 August 2013
Available online 3 September 2013

Keywords:
Nano-ferrites
Magnetic properties
Dielectric properties
GHz frequency

ABSTRACT

Magnesium ferrite ($MgFe_2O_4$) nano-structures doped with Ni–Co at magnesium and iron sites respectively were fabricated by the micro-emulsion method and characterized by the X-ray diffraction (XRD), fourier transform infrared spectroscopy (FTIR), vibrating sample magnetometer (VSM) and dielectric measurements. The analysis of XRD patterns confirm the single phase spinel structure and the crystallite size calculated by Scherer's formula lies in the range of 15–26 nm. The spectral studies elucidate the characteristic feature of spinel phase. The real and imaginary parts of dielectric constant and dielectric loss exhibit peaking behavior. The dielectric properties have been explained on the basis of Debye-type relaxation phenomenon in accordance with Koop's phenomenological theory. The increase in the tendency of saturation magnetization is consistent with the enhancement of crystallinity. The crystallite size is small enough to obtain considerable signal to noise ratio in the recording media. The optimized dielectric and magnetic parameters suggest that the material with composition $Mg_{0.6}\,Ni_{0.4}\,Co_{0.4}\,Fe_{1.6}O_4$ may be used for applications in recording media and microwave devices.

1. Introduction

Nano-ferrites have shown a growing interest in recent years due to their specific electromagnetic properties. Spinel ferrites are currently used as key materials for the advancements in information storage devices and ferro-fluid technology [1]. The dielectric properties of nano-ferrites are influenced when the crystallite size approaches the critical value, below which every crystallite is treated as single domain. Hence this realizes that the physical and chemical properties of these ferrites in the nano-regime are in general dramatically different from those of the bulk counter parts and that the nano-materials exhibit new cross over phenomena. The modern data storage requirement needs smaller crystallite size [2]. Magnesium ferrite is one of the most important ferrites. The doped magnesium nano-ferrites found considerable applications in transformers, ac power distributors, magnetic recording as a magnetic heads, and magnetic sensors [3]. The basis for variety of applications is related to the verity of transition metal cations, which can be incorporated in to the spinel lattice of the parent magnetic structure. The origin of magnetic properties of these nano-ferrites is spin magnetic moment of the unpaired 3d electrons of the transition element occupied by the super exchange interaction through oxygen ions separation. The magnetic properties such as saturation magnetization are strongly dependent on the distribution of cations, type of dopants and the crystallite size [4]. The influence of metal ion substitution such as Zn [5], Cd [6], Al [7], Cu [8], Cr [9] and Ge [10] on various structural, magnetic, electrical and dielectric properties of $MgFe_2O_4$ have been reported in the literature. In the present work, we have investigated the effects of Ni^{2+}–Co^{2+} substitution for Mg^{2+} and Fe^{3+} in magnesium based spinel ferrites ($Mg_{1-x}\,Ni_x\,Co_y\,Fe_{2-y}O_4$) synthesized by micro-emulsion method. The results show that the coercivity of all the substituted samples was found to be a few hundred oersteds which is one of the necessary conditions for recording media [11].

* Corresponding author. Tel.: +92 345 5411391.
E-mail addresses: farooqsi_warsi@yahoo.com, farooq.warsi@iub.edu.pk (M.F. Warsi).

0925-8388/$ - see front matter © 2013 Elsevier B.V. All rights reserved.
http://dx.doi.org/10.1016/j.jallcom.2013.08.114

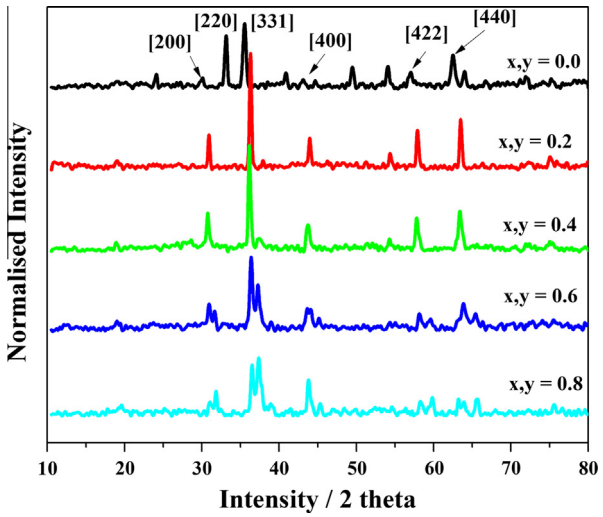

Fig. 1. X-ray diffraction patterns for Mg_{1-x} Ni_x Co_y $Fe_{2-y}O_4$ nano-ferrites.

2. Experimental details

The Mg_{1-x} Ni_x Co_y $Fe_{2-y}O_4$ (where x, y = 0.0, 0.2, 0.4, 0.6 and 0.8) nano-ferrites of stoichiometric composition were prepared using $MgSO_4{\cdot}7H_2O$, $NiCl_2{\cdot}6H_2O$, $CoCl_2{\cdot}6H_2O$ and Fe $(NO_3)_2{\cdot}9H_2O$ as starting materials by micro-emulsion method The detail study about synthesis is already published elsewhere [12]. The chemical structure of ferrite nano-powders was investigated by the X-ray diffraction technique. The X-ray diffraction patterns were recorded using Cu Kα radiation (λ = 1.5406 Å) at room temperature. The X-ray diffraction patterns were recorded in the range 10–80°, 0.20/min in steps of 0.02 shown in Fig. 1. The FTIR spectra were recorded using Perkin Elmer Spectrum FTIR Spectrometer. The samples were prepared using KBr: ferrites with 100:1 ratio. The FTIR spectra were recorded in the range of 400–4000 cm^{-1} at room temperature. The magnetic hysteresis were measured at room temperature using vibrating sample magnetmeter (VSM). The frequency dependent dielectric measurements were made in the range 100 MHz to 3 GHz using an HP 4192 Impedance analyzer.

3. Results and discussion

3.1. Structural properties

The X-ray diffraction patterns of Mg_{1-x} Ni_x Co_y $Fe_{2-y}O_4$ nano-ferrites are shown in Fig. 1. The patterns correspond to well defined crystalline FCC phase and confirm the single spinel structure without any ambiguous reflection. The reflections from the diffraction planes (200), (220), (311), (400), (422) are shown by all samples [13]. Experimentally observed d spacing values and relative intensities of the diffraction peaks are in well agreement with the crystalline cubic spinel form of the magnesium ferrite ICDD # 01-073-2410). The plane (311) indicates maximum intensity for all samples. The intensity of the (220) is more sensitive to the cations on tetrahedral sites [14] and the intensity of (400) plane is sensitive to cations on the octahedral sites [15,16]. It has been reported earlier that Mg^{2+} ions have a strong preference to occupy B sites and partially occupy A sites [17]. The observed intensities of the above two planes are found to decrease by the substitution of Co^{2+} and Ni^{2+} cations. The decrease in the intensity of the (400) plane indicate that the substitution of Co^{2+} and Ni^{2+} ions takes place at B-site, i.e. the octahedral site on the (400) plane. Hence, it is expected that most of the replacement of substituted cations (Co^{2+}, Ni^{2+}) occur on the octahedral sites. The lattice parameter is obtained by fitting seven diffraction peaks using standard Nelson–Riley refinement method [18]. The calculated value of lattice parameter 8.383 Å for $MgFe_2O_4$ nano-ferrites agrees quite well with literature values of 8.384 Å [19], 8.387 Å [20] and 8.372 Å [21] for $MgFe_2O_4$ nano-ferrites. It is evident from the Table 1 that the lattice parameter increases smoothly with increase in Ni–Co contents. The increase in lattice parameter can be explained on the basis of difference in ionic radii of Ni–Co. The larger ionic radii of Co (0.72 Å) and Ni (0.69 Å) replaced the smaller ionic radii of Fe^{3+} (0.67 Å) and Mg^{2+} (0.66 Å), consequently the lattice parameter increased due to expansion in the unit cell. The XRD patterns indicated that the synthesized powders contain nano-sized crystallites. The crystallite size is estimated by using the Scherrer's formula.

$$D = \frac{0.9\lambda}{\beta \cos\theta} \tag{3.1}$$

where D is the crystallite size, λ is the wave length of X-ray (1.5406 Å), β is the full width at half maximum, and θ is the angle of diffraction. The average crystallite size (Table 1) of the Co–Ni substituted samples is found in the range 15–26 nm. The X-ray density of the samples is calculated by the relation:

$$\rho_x = \frac{8M}{Na^3} \tag{3.2}$$

where M is the molecular weight of the sample, N is avogadro's number and a^3 volume of the cubic unit cell. The measured density is calculated by using the relation:

$$\rho_m = \frac{M}{V} = \frac{M}{\pi r^2 t} \tag{3.3}$$

where M is the mass, r is the radius, and t is the thickness of the pellet. The X-ray density increases from the 4.51 to 5.21 g/cm^3 while measured density varies from 2.57 to 4.02 with the substitution of Co–Ni contents.

3.2. FT-IR spectroscopy

The IR spectra show the bands arising from inter atomic vibrations. The structural changes brought about by the metal ions strongly influenced the lattice vibrations. The lattice vibrations also depend on the cations mass, the cation oxygen and the bonding force. Fig. 2 shows the representative room temperature FTIR spectrum of Mg_{1-x} Ni_x Co_y $Fe_{2-y}O_4$ nano-ferrites (x, y = 0.6). The representative spectrum of these as synthesized nano-ferrites obtained at room temperature manifest absorption peaks located at about 424, 435.9, 454.7, 549.3, 1077.4, 1652.1 and 3249.9, in the range of 400–4000 cm^{-1}. The inset indicates two absorption bands

Table 1
Crystallite size (D), lattice parameter (a), cell volume (V_{cell}), X-ray density (ρ_x), measured density (ρ_m) and porosity (P%) of Mg_{1-x} Ni_x Co_y Fe_{2-y} O_4 (x = 0.0–1.0, y = 0.0–1.0) nano-ferrites.

Parameters	x = 0 y = 0	x = 0.2 y = 0.2	x = 0.4 y = 0.4	x = 0.6 y = 0.6	x = 0.8 y = 0.8
Lattice constant (a) (Å)	8.383	8.386	8.390	8.393	8.395
Cell volume (V_{cell}) (Å^3)	589.11	589.74	590.59	591.22	591.65
Measured density (ρ_m) (g cm^{-3})	2.57	2.78	2.82	3.02	4.02
X-ray density ($\rho_{X\text{-ray}}$) (g cm^{-3})	4.51	4.68	4.86	5.03	5.21
Crystallite size (D) (nm)	16.10	17.27	26.19	15.53	15.94

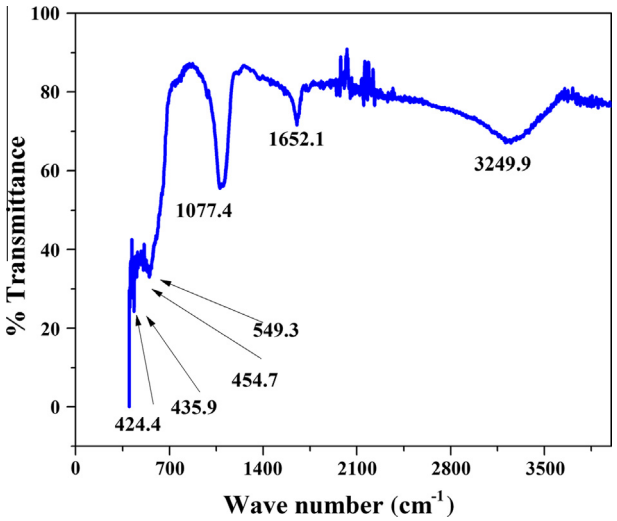

Fig. 2. FTIR spectra for Mg_{1-x} Ni_x Co_y $Fe_{2-y}O_4$ nano-ferrites (x, y = 0.6).

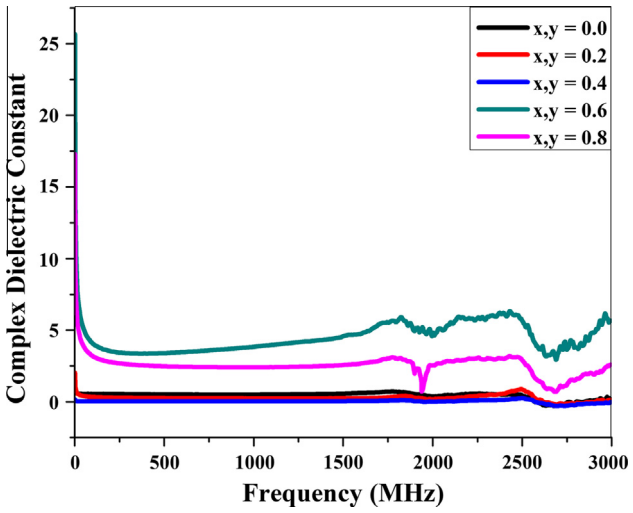

Fig. 4. Complex dielectric constant for Mg_{1-x} Ni_x Co_y $Fe_{2-y}O_4$ nano-ferrites.

which is a common feature of all ferrites [22]. The two main absorption bands (ν_1) and (ν_2) corresponding to the stretching vibration of the tetrahedral and octahedral sites are around 550 and 400 cm^{-1}, respectively [23]. In Fig. 2 the bands observed 424, 436, 454 cm^{-1} assigned to octahedral group complexes [24] while the band 549 cm^{-1} attributed to the tetrahedral group complexes. The tetrahedral bands are shifted from lower bands to higher bands i.e., 520–558 cm^{-1}, that can be ascribed to the shifting of Fe^{3+} ions towards oxygen ion on the tetrahedral site which decreases Fe^{3+}–O^{2-} distances. The band at 1077.4 cm^{-1} is attributed to the formation of Co substituted spinel ferrites [25]. The band at 1652.1 cm^{-1} is ascribed to the presence of absorbed water (H–O–H) [6]. The absorption band at 3249.9 attributed to the stretching mode of H–O–H bending vibration of free or absorbed water which implies that the hydroxyl groups are retained in ferrites [26]. Thus a combination of XRD data with the frequency and position of absorption bands in FTIR spectra has a close agreement to support our conclusions.

3.3. Dielectric properties

The dielectric properties of ferrites nano-ferrites depend upon the method of preparation, chemical composition, crystallite size and cation distribution. The frequency dependent dielectric constant, complex dielectric constant and dielectric loss of Mg_{1-x} Ni_x Co_y $Fe_{2-y}O_4$ nano-ferrites (x, y = 0.0, 0.2, 0.4, 0.6, 0.8) have been studied at room temperature. The Figs. 3 and 4 depict the variation of real and complex part of the dielectric constant as a function of an applied ac field in the frequency range of 100 MHz to 3 GHz. It can be seen that all the compositions exhibit dielectric dispersion where both the dielectric constant and complex dielectric constant decrease as the frequency increase from 100 Hz to 3 GHz. Initially, the dielectric constant decreases rapidly in the low frequency region but in the high frequency region its value becomes so small that it becomes almost independent of applied field. The dispersion of ferrites in the low frequency region is due to space charge effect [27]. The complex dielectric constant decreases more rapidly as compared to the real part of the dielectric constant. The observed behavior of dielectric dispersion in ferrites can be explained on the basis of Maxwell–Wagner model and Koops phenomenological theory [28–30]. The dielectric medium consist of well conducting grains which are separated by poorly conducting grain boundaries. In the low frequency region grain boundaries are effective while, grains are effective at higher frequencies. The grain boundaries are formed in the sintering process due to oxidation of crystallites in a porous material as a result of their direct contact with the firing atmosphere. The frequency independent behavior of all the samples at higher frequencies of an applied electrical field is due to the charge carriers which are responsible for various mechanisms of polarization and that lag behind the applied alternating field. As a result the charge carriers cannot follow the changes in the applied electric field over a certain frequency range, as the frequency increases [31].

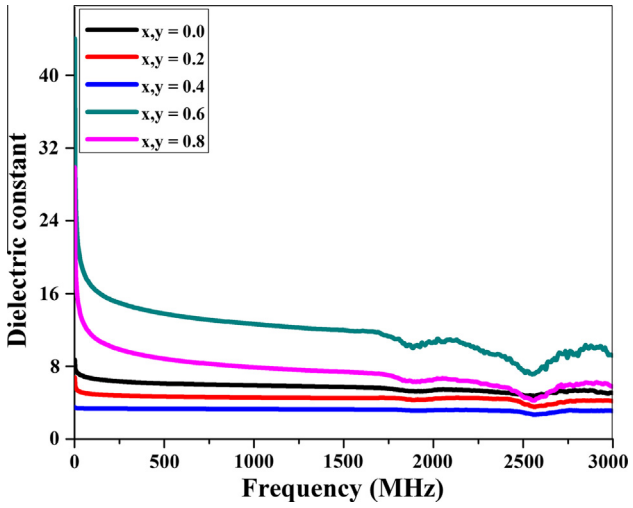

Fig. 3. Dielectric constant Mg_{1-x} Ni_x Co_y $Fe_{2-y}O_4$ nano-ferrites.

The dielectric constant becomes constant at 1.75 GHz after attaining a minimum value. In the high frequency region (~GHz) two peaks have been observed around 2 GHz and 2.5 GHz. This type of peaking behavior (relaxation peaks) is observed in ferrites due to Debye-type relaxation and is observed when the jumping frequency of the Fe^{+2} and Fe^{+3} ions is exactly equal to the frequency of applied field [32]. The dielectric constant decreases as the concentration of Ni–Co increased from 0.0 to 0.4 and for $x \geqslant 0.6$ it increased. The decreased in the dielectric constant is explained as follows: The conduction mechanism in Mg_{1-x} Ni_x Co_y $Fe_{2-y}O_4$ spinel ferrites takes place due to electron hopping between Fe^{3+} and Fe^{2+} ions at octahedral (B-site) and hole hopping between Ni^{2+} and Ni^{3+} ions [33]. In the spinel lattice, Fe^{3+} ions reside on both A- and B-sites while Co^{2+} and Ni^{2+} ions prefer to occupy B-sites. After the substitution of Ni^{2+} and Co^{2+} ions by Mg^{2+} and Fe^{3+} ions, some of the Mg^{2+} ions occupy A-sites in the spinel lattice

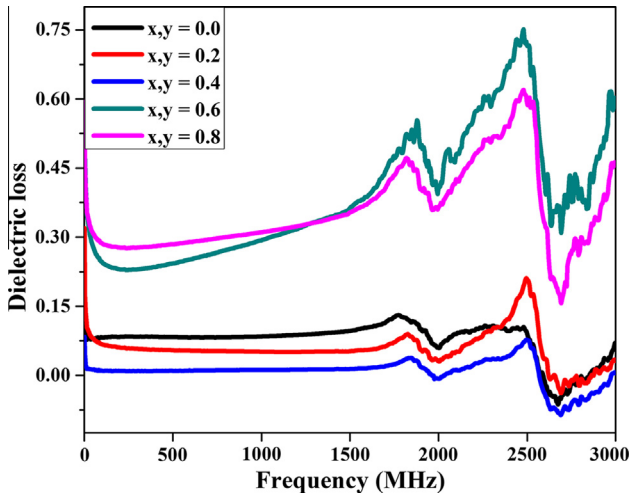

Fig. 5. Dielectric loss as a function of frequency for Mg_{1-x} Ni_x Co_y $Fe_{2-y}O_4$ nano-ferrites.

displacing Fe^{3+} ions from there. These displaced Fe^{3+} ions migrate from A-site to B-site and thus increase the concentration of Fe^{3+} ions at B-site. Thus hopping conduction further enhances dielectric polarization at the grain boundary, consequently dielectric constant decreases [34]. For higher concentrations $x \geqslant 0.6$ no more Fe^{3+} ions migrate at B-site and the presence of Co^{2+} ions obstruct the hopping conduction, hence the dielectric polarization reduced at the grain boundaries.

The Fig. 5 depicts the variation of dielectric loss as a function of an applied ac field in the frequency range of 100 MHz to 3 GHz. The dielectric loss measures the loss of electrical energy from the applied electric field into the samples at various frequencies. It is observed that the tan loss shows a decreasing trend with increase in frequency. However, In case of x, $y = 0.6$ and 0.8, it increases with an increase in frequency thus normal behavior is deviated. After reaching the frequency of 1.5 GHz, two peaks are observed for each sample. The dielectric loss is more at high frequencies because of increase in interruption to the passage of electric field through nano-crystalline material due to its interaction with the oscillating majority charge carriers of the dielectric medium.

3.4. Magnetic properties

The magnetic hysteresis loops obtained for the present nano-ferrites are shown in Fig. 6. The narrow hysteresis loops for Mg_{1-x} Ni_x Co_y $Fe_{2-y}O_4$ (where x, $y = 0.0$, 0.2, 0.4, 0.6 and 0.8) revealed the soft magnetic nature of these nano-ferrites. All the curves indicate normal behavior, the saturation magnetization

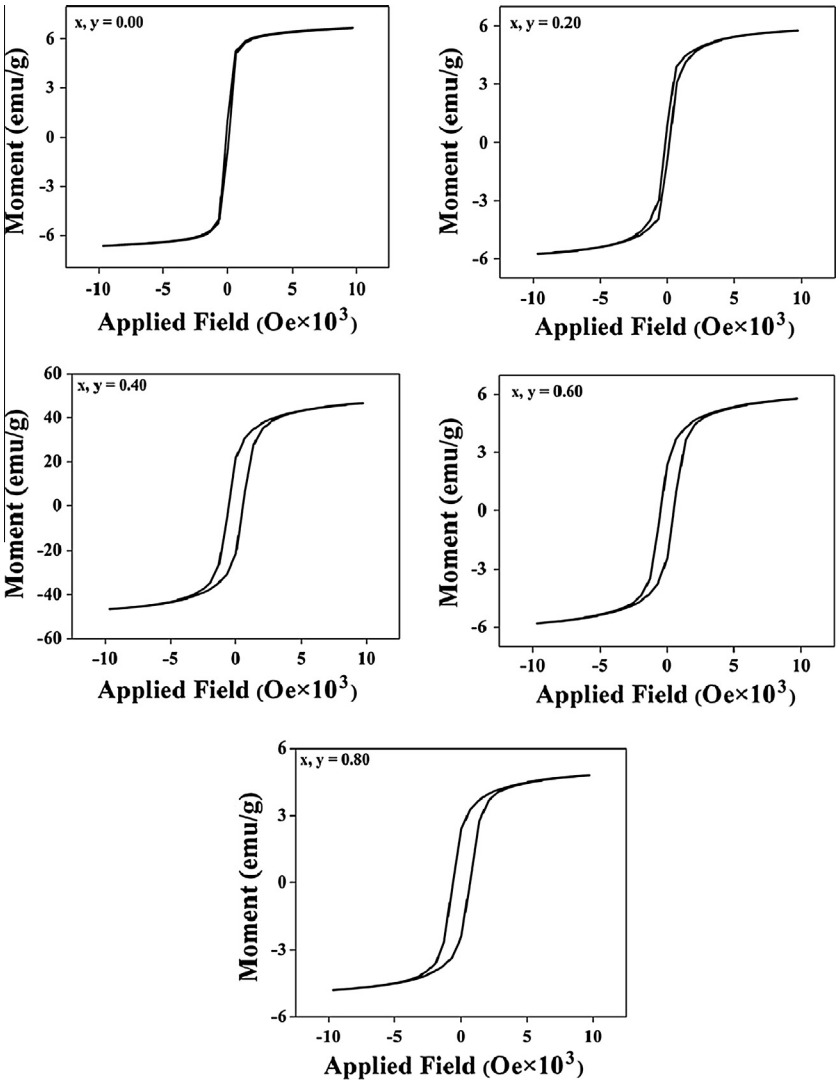

Fig. 6. MH loops of Mg_{1-x} Ni_x Co_y $Fe_{2-y}O_4$ nano-ferrites (x, $y = 0$ to x, $y = 0.80$).

Table 2
Various magnetic parameters for Mg_{1-x} Ni_x Co_y Fe_{2-y} O_4 (x = 0.0–0.8, y = 0.0–0.8) nano-ferrites.

Magnetic parameters	x = 0 y = 0	x = 0.2 y = 0.2	x = 0.4 y = 0.4	x = 0.6 y = 0.6	x = 0.8 y = 0.8
Magnetization (M_s) (emu/g)	4.82	5.75	19.44	4.13	4.18
Coercivity (H_c) (G)	95.544	141.83	545.32	486.03	629.46
Retentivity (M_r) (emu/g)	0.54	0.83	6.53	1.32	1.85
Magnetic moment (bohr magneton)	0.17	0.21	0.75	0.16	0.17

increased win the increase in applied magnetic field. The magnetic parameters such as saturation magnetization (M_s) and coercivity (H_c) are obtained from hysteresis loops. The saturation magnetization for each sample was determined by the magnetization curve at H_{max}. The values of saturation magnetization (M_s), coercivities (H_c) and magnetic moments (n_B) for different Ni–Co substituted nano-particles are listed in Table 2 and these values are comparable with [35–38] The magnetic moment per formula unit in Bohr magneton (μ_B) is calculated by using the formula [39].

$$\eta_B = \frac{M \times M_S}{5585} \tag{3.4}$$

where M is the molecular weight of a particular nano-ferrite and M_s is the saturation magnetization (emu/g). The magnitude of applied field required to reach saturation depends on the size of the nano-materials [40]. In the present work most of the compositions exhibit lower magnetization and higher coercivity values. Similar magnetization results for nano-materials are available in the literature [37]. The Ni–Co dependence of saturation magnetization coercivity and remanance (M_r) is shown in Fig. 7. The Fig. 7 exhibit that an increase in Ni–Co concentrations increase H_c 95–629 Oe (for x, y = 0–0.8) and M_s increase 4.82–19.44 emu/g (upto x, y = 0.4) and there after M_s decreases. In $MgFe_2O_4$ Mg possess no magnetic moment and compound's total magnetic moment is due to the uncompensated magnetic moments of ferric ions [41]. The increase in M_s can be attributed to the larger magnetic moments of Ni^{2+} (2.83 μ_B) as compared to the Mg^{2+} (0 μ_B) at the octahedral site [42,43]. Also, the value of saturation magnetization (M_s) increases with an increase in crystallinity which in turn increases with an increase in crystallite size [21] and cation distribution [44]. The decrease in saturation magnetization can be explained as follows: The surface affects can lead to the decrease of saturation magnetization for oxide nano-materials. The existence of magnetically dead layer on the material's surface and some degree of spin canting in the whole volume of the crystallite could be the explanation of the additional decrease in saturation magnetization [45]. The increase in coercivity is ascribed to the much larger magnetocrystalline anisotropy of the co^{2+} ion due to strong L–S coupling and three unpaired electrons. The ferrite materials which are useful in high density recording applications require magnetization as much as possible and coercivity value high enough to 600 Oe [11]. In the present work, the improved saturation magnetization (19.44 emu/g) and coercivity values (~600 Oe) are obtained. So the composition $Mg_{0.6}Ni_{0.4}Co_{0.4}Fe_{1.6}O_4$ can be used for applications in recording media

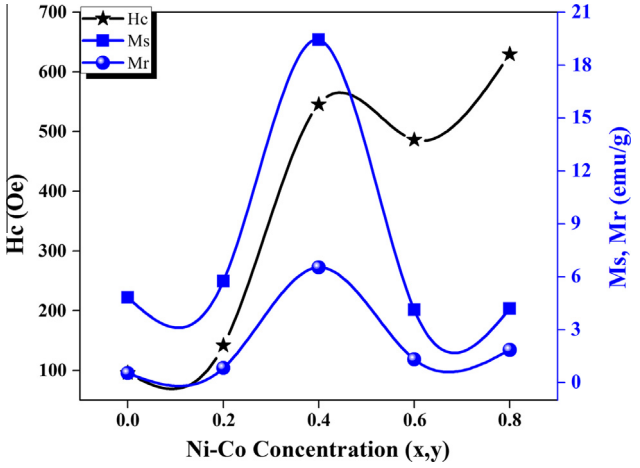

Fig. 7. The variation of coercivity (H_c), saturation magnetization (M_s) and remanence (M_r) as a function of Ni–Co contents.

4. Conclusions

Mg_{1-x} Ni_x Co_y $Fe_{2-y}O_4$ nano-ferrites were successfully synthesized with various crystallite sizes using micro-emulsion technique. The spectral and XRD analysis revealed spinel structure of these nano-ferrites and the calculated crystallite size (15–26 nm) is useful in obtaining the suitable signal to noise ratio in the recording media. The dielectric constant decreases from 5.87 to 3.26 and dielectric loss decrease from 8.4×10^{-2} to 1.1×10^{-2} at 1.0 GHz with increase in dopant concentration up to x = 0.4.

It is observed that the substitution of Ni–Co in Mg_{1-x} Ni_x Co_y $Fe_{2-y}O_4$ nano-ferrites leads to an increase in coercivity (H_c) from 95 to 545 Oe and saturation magnetization (M_s) from 4.82 to 19.44 emu/g up to x = 0.4. The smaller values of dielectric constant and dielectric loss while increase in coercivity and saturation magnetization suggest that the sample with dopant concentration x = 0.4 is suitable for microwave devices and recording media.

Acknowledgements

The authors would like extend their sincere appreciation to the Deanship of Scientific Research at King Saud University for its funding of this research through the Research Group Project no RGP-VPP-312. We are also thankful, The Islamia University of Bahawalpur-63100 and Higher Education Commission of Pakistan for financial support under Project No: PM-IPFP/HRD/HEC/2011/2264, Materials Research Laboratory (MRL), University of Peshawar for dielectric measurements, Quaid-e-Azam University Islamabad for XRD and FTIR measurements, and institute of Solid State Physics (University of the Punjab, Lahore) for magnetic measurements.

References

[1] M.J. Iqbal, Z. Ahmad, T. Meydan, Y. Melikhov, J. Appl. Phys. 111 (2012) 033906–033907.
[2] K.M. Batoo, S. Kumar, C.G. Lee, Alimuddin, Curr. Appl. Phys. 9 (2009) 826–832.
[3] M.A. Khan, M.U. Islam, M. Ishaque, I.Z. Rahman, J. Alloys Comp. 519 (2012) 156–160.
[4] J. Smiths, Magnetic Properties of Materials, Mc Graw Hill, 1971.
[5] K.A. Mohammed, A.D. Al-Rawas, A.M. Gismelseed, A. Sellai, H.M. Widatallah, A. Yousif, M.E. Elzain, M. Shongwe, Phys. B: Condensed Matter 407 (2012) 795–804.
[6] M. Kaur, S. Rana, P.S. Tarsikka, Ceram. Int. 38 (2012) 4319–4323.
[7] K. Modi, H.H. Joshi, J. Mater. Sci. Lett. 17 (1998) 741–743.
[8] A. Pradeep, G. Chandrasekaran, Mater. Lett. 60 (2006) 371–374.
[9] P.P. Hankare, V.T. Vader, N.M. Patil, S.D. Jadhav, U.B. Sankpal, M.R. Kadam, B.K. Chougule, N.S. Gajbhiye, Mater. Chem. Phys. 113 (2009) 233–238.
[10] D.R. Sagar, C. Prakash, P. Kishan, Solid State Commun. 68 (1988) 193–195.
[11] D.S. Mathew, R.-S. Juang, Chem. Eng. J. 129 (2007) 51–65.
[12] A. Mahmood, M.F. Warsi, M.N. Ashiq, M. Sher, Mater. Res. Bull. 47 (2012) 4197–4202.

[13] W.B. Cross, L. Affleck, M.V. Kuznetsov, I.P. Parkin, Q.A. Pankhurst, J. Mater. Chem. 9 (1999) 2545–2552.
[14] D. Varshney, K. Verma, A. Kumar, J. Mole. Struct. 1006 (2011) 447–452.
[15] B.P. Ladgaonkar, A.S. Vaingankar, X-ray diffraction investigation of cation distribution in $Cd_xCu_{1-x}Fe_2O_4$ ferrite system, Mater. Chem. Phys. 56 (1998) 280–283.
[16] C.S. Narasimhan, C.S. Swamy, Phys. Status Solidi (a) 59 (1980) 817–826.
[17] R.G. Kulkarni, H.H. Joshi, Solid State Commun. 53 (1985) 1005–1008.
[18] B.D. Cullity, Elements of X-Ray Diffract, Addison Wesley, USA, 1978.
[19] M. Manjurul Haque, M. Huq, M.A. Hakim, Phys. B: Condensed Matter 404 (2009) 3915–3921.
[20] V.K. Mittal, P. Chandramohan, S. Bera, M.P. Srinivasan, S. Velmurugan, S.V. Narasimhan, Solid State Commun. 137 (2006) 6–10.
[21] S. Maensiri, M. Sangmanee, A. Wiengmoon, Nanoscale Res. Lett. 4 (2009) 221–228.
[22] C.G. Ramankutty, S. Sugunan, Appl. Catal. A: Gen. 218 (2001) 39–51.
[23] J. Liu, T. Xu, M. Gong, F. Yu, Y. Fu, J. Memb. Sci. 283 (2006) 190–200.
[24] A. Maqsood, K. Khan, M. Anis-ur-Rehman, M.A. Malik, J. Alloys Comp. 509 (2011) 7493–7497.
[25] P. Pulišová, J. Kováč, A. Voigt, P. Raschman, J. Magn. Magn. Mater. 341 (2013) 93–99.
[26] P. Priyadharsini, A. Pradeep, P.S. Rao, G. Chandrasekaran, Mater. Chem. Phys. 116 (2009) 207–213.
[27] R. Laishram, S. Phanjoubam, H.N.K. Sarma, C. Prakash, J. Phys. D: Appl. Phys. 32 (1999) 2151.
[28] C.G. Koops, Phys. Rev. 83 (1951) 121–124.
[29] J.C. Maxwell, Electricity and magnetism, Electric. Magn. 1 (1873) 328–330.
[30] K.W. Wagner, Ann. Phys. 40 (1913) 817–855.
[31] M.A. El Hiti, J. Magn. Magn. Mater. 192 (1999) 305–313.
[32] A.M. Abdeen, O.M. Hemeda, E.E. Assem, M.M. El-Sehly, J. Magn. Magn. Mater. 238 (2002) 75–83.
[33] M. Naeem, N.A. Shah, I.H. Gul, A. Maqsood, J. Alloys Comp. 487 (2009) 739–743.
[34] M.A. El Hiti, J. Magn. Magn. Mater. 164 (1996) 187–196.
[35] Y. Huang, Y. Tang, J. Wang, Q. Chen, Mater. Chem. Phys. 97 (2006) 394–397.
[36] K. Maaz, W. Khalid, A. Mumtaz, S.K. Hasanain, J. Liu, J.L. Duan, Physica E: Low-dimensional Syst. Nanostruct. 41 (2009) 593–599.
[37] K. Maaz, A. Mumtaz, S.K. Hasanain, M.F. Bertino, J. Magn. Magn. Mater. 322 (2010) 2199–2202.
[38] J. Azadmanjiri, Mater. Chem. Phys. 109 (2008) 109–112.
[39] R.C. Kambale, N.R. Adhate, B.K. Chougule, Y.D. Kolekar, J. Alloys Comp. 491 (2010) 372–377.
[40] J. Feng, Y. Zheng, J. Xie, Mater. Lett. 27 (1996) 219–223.
[41] A. Pui, D. Gherca, N. Cornei, Mater. Res. Bull. 48 (2013) 1357–1362.
[42] Y. Köseoğlu, M. Bay, M. Tan, A. Baykal, H. Sözeri, R. Topkaya, N. Akdoğan, J. Nanopart. Res. 13 (2011) 2235–2244.
[43] T. Sodaee, A. Ghasemi, E. Paimozd, A. Paesano Jr., A. Morisako, J. Magn. Magn. Mater. 330 (2013) 169–173.
[44] A. Pradeep, P. Priyadharsini, G. Chandrasekaran, J. Magn. Magn. Mater. 320 (2008) 2774–2779.
[45] R.H. Kodama, Magnetic nanoparticles, J. Magn. Magn. Mater. 200 (1999) 359–372.